Journal of Biomedical Optics

SPIEDigitalLibrary.org/jbo

Fast imaging of high-resolution two-dimensional effective attenuation profile from diffuse reflectance

Jorden Tse
Lian-Kuan Chen

SPIE

Fast imaging of high-resolution two-dimensional effective attenuation profile from diffuse reflectance

Jorden Tse and Lian-Kuan Chen
The Chinese University of Hong Kong, Department of Information Engineering, Hong Kong

Abstract. Biological tissue is non-homogeneous in nature. It is difficult to measure its optical properties due to non-uniformity throughout the tissue being tested. To obtain the spatial distribution of optical parameters, conventional approaches use an array of light sources and detectors to reconstruct the image, thus, there is very limited spatial resolution. In contrast, solutions that provide high resolution have a high computational complexity. In this paper, we propose a fast, simple scheme to resolve the effective attenuation profile from the spatial diffuse reflectance. Rather than giving one single value for the absorption and reduced scattering coefficients, a novel algorithm is proposed for the reconstruction of an effective attenuation profile in 2-dimension from a diffuse reflectance curve. This technique is applied to the reconstruction of a 2-D effective attenuation profile. By obtaining the diffuse reflectance image from a camera and using the algorithm developed here, fast imaging of the effective attenuation profile with relatively high spatial resolution can be achieved.
[DOI: 10.1117/1.JBO.17.4.046005]

Keywords: diffuse optics; near-infrared spectroscopy; diffuse optical tomography; tissue imaging.

Paper 11286 received Jun. 7, 2011; revised manuscript received Feb. 2, 2012; accepted for publication Feb. 2, 2012; published online Apr. 6, 2012.

1 Introduction

When light propagates through biological tissue, photons are absorbed, scattered, reflected or refracted. The absorption of a photon and how energy is transferred relate to the nature of the matter that interacts with light.[1] The spectral intensity of diffuse light in a tissue reveals information about its physical density and chemical composition. Many applications and algorithms have been developed to resolve the optical properties from light diffusion and, in turn, the chemical composition and physical properties can be deduced by spectroscopy.[2–5] For instance, the absorption properties of red and near-infrared light are employed to determine the hemoglobin composition and oxygen saturation of blood.[2] The spatial blood oxygen distribution provides information on blood flow in functional near-infrared spectroscopy.[3,4]

Theoretically, the light diffusion process and diffuse reflectance with given optical properties can be predicted using Monte Carlo (MC) simulation or the diffusion equation.[6,7] The modeling of diffuse light in biological tissue is commonly known as the forward problem. While the MC simulation and the diffusion equation give an accurate and efficient solution to the problem, in practice, we are more interested in finding the chemical composition and physical structure of biological tissue from the diffusion pattern and response. This is referred to as the inverse problem. Much prior work has been done on deriving optical properties from the measurements of diffuse reflectance or transmittance using photo-detector array or CCD cameras.[8–10] Diffuse reflectance is often recorded as the spatial distribution or temporal impulse response of the diffuse photons.[11–13] Optical properties, such as reduced scattering coefficient and absorption coefficient, can be resolved by solving the diffusion equation or by comparison with the solution of the forward problem.[5,14,15]

To obtain the 2-D effective attenuation profile of a non-homogeneous biological tissue, the common practice is to use an array of detectors and light sources to segment the tissue into several homogeneous parts for measurement. In Ref. 11, a low resolution 2-D reconstruction of muscle oxygenation was obtained from the resolved absorption parameters in each probe.[11] In spatially resolved systems, it is usually assumed that the tissue optical properties are uniform in each section covered by a light source and detector. Due to the non-homogeneous nature of biological tissue, this assumption of uniform optical properties may lead to enormous errors. Problems may occur when some hetero-structures, such as blood vessels, are located in the optical path between the light source and detector. Biological tissue absorption imaging is normally accomplished using a CCD camera.[16] It has been reported that the subcutaneous veins can be visualized using a near-infrared light source and camera.[17] However, the absorption value and the captured light intensity would not be accurately related due to the tissue geometry and the nonlinearity between the diffuse light intensity and the absorption value.[18] Recent studies have revealed that diffuse optical tomography (DOT) and modulated imaging create a good 3-dimensional (3-D) reconstruction of biological tissue.[19,20] On the other hand, the high computational complexity in processing a huge amount of data of over 10^7 measurements in DOT still hinders its application for real-time high resolution imaging.[19] In view of the trade-off between spatial resolution and computational complexity, diffuse optics based imaging is less practical than other imaging techniques such as ultrasonography.

In this paper, we propose a fast and simple solution to the problem of imaging a non-homogeneous medium by simplifying the steady-state diffusion approximation for diffuse reflectance.[7] We will demonstrate that from the diffuse reflectance

Address all correspondence to: Jorden Tse, The Chinese University of Hong Kong, Room 827, Sin Hang Engineering Building, Hong Kong. Tel: +852 26098479; E-mail: jorden@ie.cuhk.edu.hk.

0091-3286/2012/$25.00 © 2012 SPIE

along a line originating from the light source, we can resolve the effective attenuation profile rather than just a single value, as in previous applications.[10] By employing a simplified diffuse reflectance approximation model, we can solve the effective attenuation value from the spatial diffuse reflectance which describes the reflectance, R_d, at a distance r from the light source. We will show that the effective attenuation profile can be obtained by resolving the value of effective attenuation on every r. Our simulations and experiments will demonstrate that by analyzing eight diffuse reflectance images, we are able to resolve the 2-D attenuation image for a biological tissue, of size 4 cm × 4 cm, in a few seconds on a personal computer with a 2.4-GHz single-core CPU.

2 Model and Algorithm

2.1 *Simplified Diffusion Approximate Model*

The optical property of biological tissue is usually described by its absorption coefficient μ_a and reduced scattering coefficient μ_s'. The diffuse reflectance can be calculated with the MC simulation or the diffusion equation. Equation (1) shows the diffusion approximation for the diffuse reflectance, R_d, at a distance r from the light source:[21]

$$R_d(r) = a' \frac{z'(1+\mu_{\text{eff}}\rho_1)\exp(-\mu_{\text{eff}}\rho_1)}{4\pi\rho_1^3} + a' \frac{(z'+4D)(1+\mu_{\text{eff}}\rho_2)\exp(-\mu_{\text{eff}}\rho_2)}{4\pi\rho_2^3}, \quad (1)$$

where transport albedo $a' = \mu_s'/(\mu_s' + \mu_a)$,
diffusion coefficient $D = [3(\mu_a + \mu_s')]^{-1}$,
effective attenuation $\mu_{\text{eff}} = \sqrt{\mu_a/D}$,
transport mean free path $z' = (\mu_a + \mu_s')^{-1}$,
$\rho_1 = \sqrt{r^2 + z'^2}$ and
$\rho_2 = \sqrt{r^2 + (z' + 4D)^2}$.

With the assumption of the diffusion equation being isotropic scattering and large in transport albedo, the result from Eq. (1) differs from the experimental result and the MC simulation at small r.[7] Previous simulation studies have shown that the incident angle[22] and width[23] of the light beam can alter the diffuse reflectance. Nonetheless, Eq. (1) gives a close approximation of R_d in homogeneous medium in cases when a' is close to 1. The solving of μ_{eff} from R_d is commonly known as the inverse problem and the solution to Eq. (1) is discussed in Ref. 24. Since the solution has a high computational complexity, our goal is to simplify the solution to the inverse problem by simplifying Eq. (1). MC simulations show that the slope of log (R_d) is steeper as μ_{eff} increases. It is proposed in Ref. 25, and has been verified by our MC simulations that the time-independent spatial diffuse reflectance of a homogeneous medium can be approximated in the form of:

$$R_d'(r) = k_1 r^{-k_2} \exp(-k_3 r) \quad (2)$$

for some positive constants k_1, k_2 and k_3, with $r > 0$. We will illustrate in the next sub-section that the simulated diffuse reflectance of a homogeneous medium agrees well with Eq. (2) for large r.

2.2 *Homogeneous Medium*

Figure 1 shows an example of the curve fitting with Eq. (2) for the diffuse reflectance from an MC simulation on a homogeneous medium with $\mu_a = 0.1$ cm^{-1} and $\mu_s' = 10$ cm^{-1}. Equation (2) with the derived constants was found to be:

$$R_d'(r) = 0.0650 r^{-2.217} \exp(-1.735 r). \quad (2a)$$

Figure 1 depicts that Eq. 2(a) fits the diffuse reflectance found by the MC simulation in most of the region, except where r is small, $r < 0.3$ cm. We repeated this curve fitting with different pairs of absorption and reduced scattering coefficient values and verified that the simulated diffuse reflectance can be fitted with Eq. (2). Here, we will show how the constants in the diffuse reflectance approximation model for homogeneous medium are derived from the first derivative of log $R_d(r)$. From Eq. (2), taking logarithm and differentiation on both sides, we have:

$$\ln R_d'(r) = \ln k_1 - k_2 \ln r - k_3 r \quad (3)$$

$$-r \frac{d \ln R_d'(r)}{dr} = k_2 + k_3 r. \quad (4)$$

By letting $y(r) = r \frac{d \ln R_d'(r)}{dr}$, one can obtain k_2 and k_3 via linear regression on y against r. The values of $\frac{d \ln R_d'(r)}{dr}$ can be found from $\ln R_d(r)$ and a number of adjacent points around r. k_1 is obtained from Eq. (3) after finding k_2 and k_3. After repeating the curve fitting with a medium of different absorption and scattering coefficients, we plot the found k_3 constant against the effective attenuation coefficient value μ_{eff} and the found k_2 constant against the transport albedo value a' in Fig. 2.

In Fig. 2(a), MC simulations were implemented with the value of μ_s' from 1 to 20 cm^{-1}, while μ_a varies from 0.1 to 1.0 cm^{-1}. For each pair of μ_a and μ_s', k_2 and k_3 were found by the aforementioned linear regression method with $r > 1.5$ cm. The plot of k_3 versus μ_{eff} in Fig. 2(a) reveals that the value of k_3 is almost equal to μ_{eff} with an average difference of 1.3%. Therefore, k_3 can be used to estimate μ_{eff}. The value of k_2 is found to be within the range of 2.0 and 2.2 when the transport albedo value $a' > 0.9$. The approximate values of

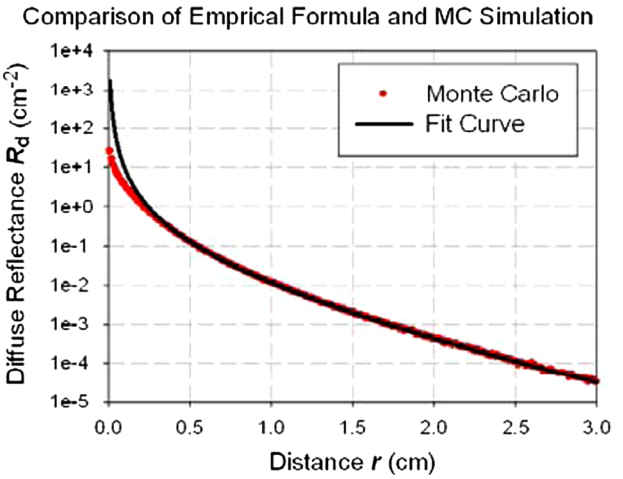

Fig. 1 Fitting diffuse reflectance using simplified diffusion approximate model.

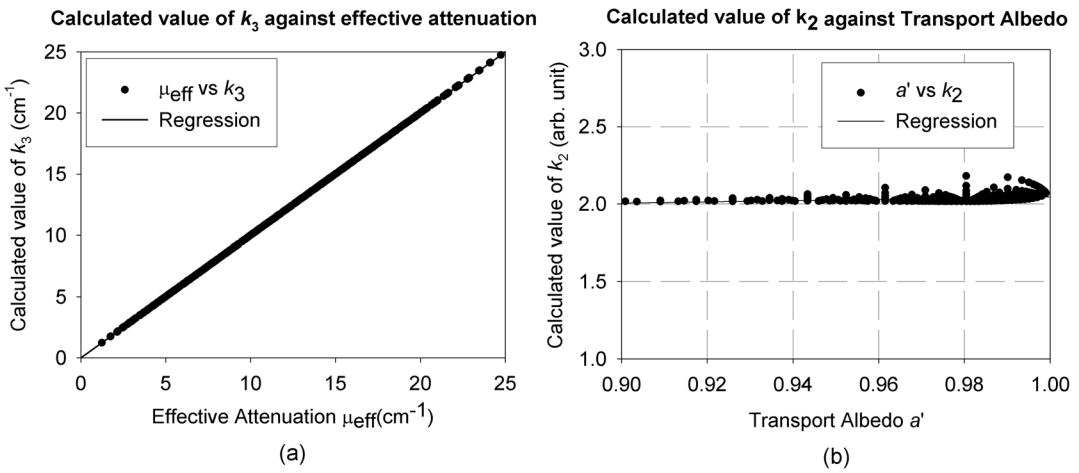

Fig. 2 (a) Plot of k_3 against μ_{eff}; (b) Plot of k_2 against a'.

k_2 and k_3 are comparable with those in Ref. 7, where $k_3 = \mu_{eff}$ and $k_2 = 2$ for large r.

2.3 *Non-Homogeneous Medium*

In reality, biological tissue does not have a constant μ_{eff} along r. Instead of applying Eq. (1) for a non-homogeneous medium, we will exploit Eq. (2) for this purpose because of its simplicity. Here, we will consider a medium which is non-homogeneous along the x-y plane and homogeneous along the depth (z) axis. A point light source is used on the origin and the simulated profile has cylindrical symmetry about the z-axis. We have shown, in Sec. 2.2, that the μ_{eff} can be resolved from the first derivative of logarithm of diffuse reflectance for homogeneous medium. For simplicity's sake, we will first assume that the transport albedo value a' is close to 1 in the non-homogeneous medium and, therefore, k_2 is relatively constant along r. Secondly, we will adopt the assumption of $k_3(r) = \mu_{eff}(r)$. With k_3 rewritten as an effective attenuation profile and k_2 being a constant, Eq. (4) becomes:

$$\frac{d \ln R'_d(r)}{dr} \approx -\frac{k_2}{r} - \mu_{eff}(r) \tag{5}$$

Equation (5) is the simplified diffusion approximation for non-homogeneous medium. It relates the first derivative of diffuse reflectance at a distance r_0 from the light source to the effective attenuation μ_{eff} at r_0. The simplified diffusion approximation for diffuse reflectance in Eq. (2) becomes:

$$R'_d(r_0) = k_1 r^{-k_2} \exp\left[-\int_0^{r_0} \mu_{eff}(r)\mathrm{d}r\right]. \tag{6}$$

In order to validate the assumption of constant k_2 and examine how well Eq. (6) will fit the diffuse reflectance of a non-homogeneous medium, several MC simulations on media with different non-uniform effective attenuation profiles were implemented. These simulated profiles were selected to investigate the diffuse reflectance modeling of Eq. (6) for various simulated μ_{eff} profiles with steep and flat slopes. The simulated spatial diffuse reflectance is then fitted with Eq. (6) and the predefined $\mu_{eff}(r)$ from the simulated profile. The fitting results are shown in Fig. 3.

Figure 3 shows that Eq. (6) fits the simulated diffuse reflectance in four cases, but not in the regions with small r or sharp changes of μ_{eff}. The diffusion process acts like a low-pass filter on the effective attenuation profile and, therefore, fast change of $\mu_{eff}(r)$ cannot be observed in the simulated diffuse reflectance. Nonetheless, it demonstrates that the simulated diffuse reflectance of a non-homogeneous medium can be fitted, showing the possibility of approximating $\mu_{eff}(r)$ from $R_d(r)$ based on Eq. (6). Derived from Eq. (5), the effective attenuation profile can be approximated from the diffuse reflectance curve for large $r(> 10z')$, as shown in Eq. (7). The transport mean free path z' is about 0.1 cm in Fig. 3.

$$\mu'_{eff}(r) \approx -\frac{d \ln R_d(r)}{dr} - \frac{k_2}{r}. \tag{7}$$

Figure 4 shows the resolved profile $\mu'_{eff}(r)$ from the simulated diffuse reflectance $R_d(r)$ as in Fig. 3. The value of k_2 is fixed at 2.15, as found in Fig. 2(b), and is assumed to be a constant. On the same graph, the respective simulated profile $\mu_{eff}(r)$ is plotted for comparison.

The reconstructed effective attenuation profiles in all four cases are low-pass filtered. The average differences between the reconstructed and input profiles are −1.60%, 2.11%, 0.257%, and 5.07% for Fig. 4(a)–4(d), respectively, where r is between 1.0 and 4.0 cm. The small average differences show the feasibility of the reconstruction algorithm. However, the resolved profile is not perfectly fitted because of the low-pass filtering of the diffusion process and a' is assumed to be a constant along the radial distance r. Apart from the region with small r, the biggest difference is found where there is a sharp change in the input profile. The simulation result shows that the value of k_2 is dependent on both a' and r. However, the assumption of constant k_2 for cases with limited r (< 4 cm) and small variation of a' (0.95 to 1.00) provides simplicity for the reconstruction algorithm and we can still achieve reconstruction that is close to the actual value. In the following section, we extend the algorithm to a 2-D case and enhance the accuracy of the algorithm by averaging the reconstructed profile from multiple light sources.

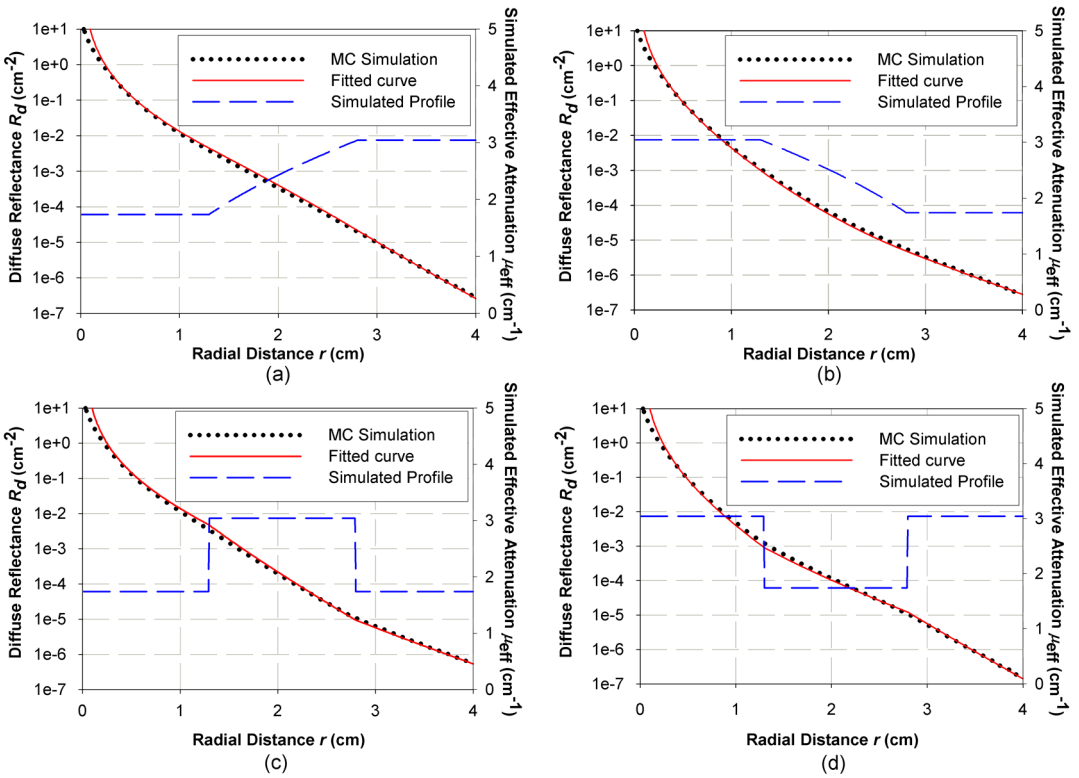

Fig. 3 Fitting diffuse reflectance using simplified diffusion approximate model for non-homogeneous media.

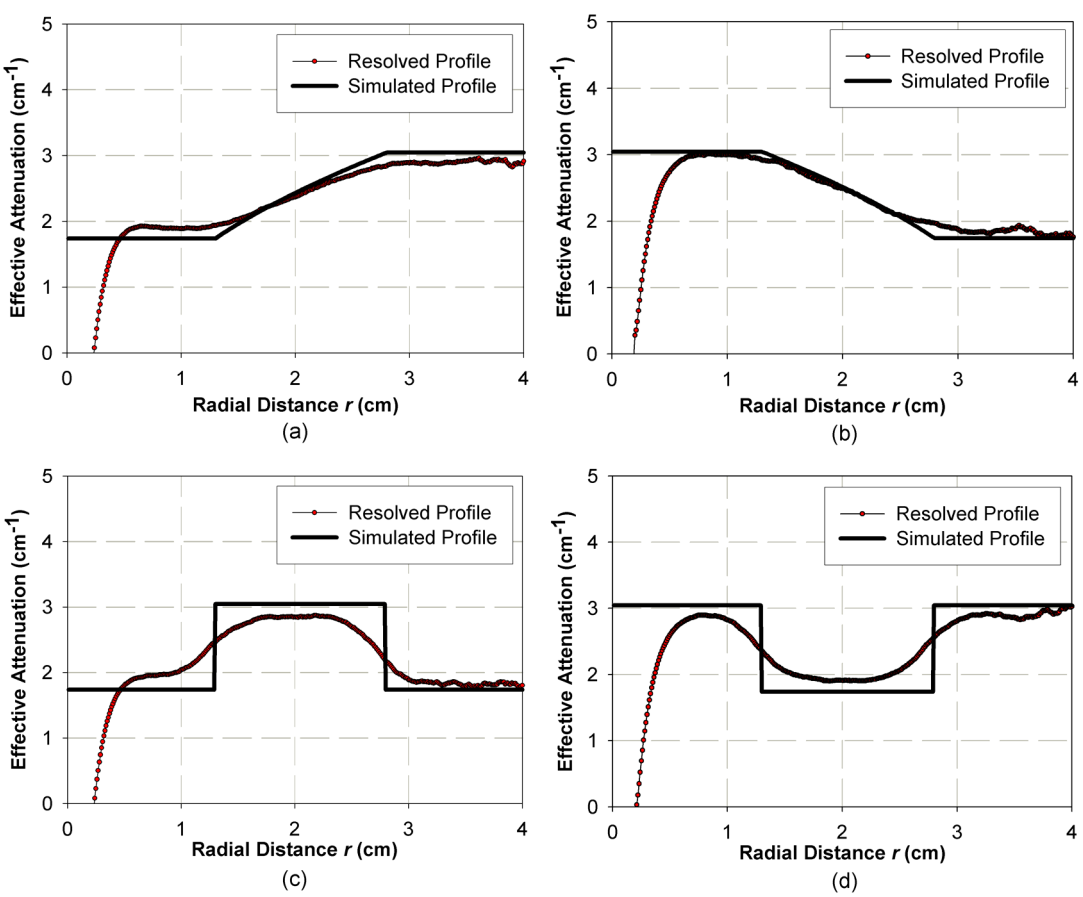

Fig. 4 Resolved effective attenuation $\mu_{eff}(r)$ profiles from diffuse reflectance $R_d(r)$.

3 2-D Reconstruction of Effective Attenuation Profile

In the above section, we proposed a simplified diffusion approximation model for diffuse reflectance and used it to reconstruct the effective attenuation profile from the diffuse reflectance. Here, we aim at developing a fast and simple solution for the 2-D profile. We use eight point light-sources, around the perimeter of a square area, in the 2-D reconstruction of an effective attenuation profile. This gives a better coverage of the invalid region with small r by single light source as shown in Fig. 4. To extend the previous algorithm to 2-D imaging, we treat each line originating from the point light source as an independent diffuse reflectance curve and solve it for the effective attenuation profile. In this section, we will demonstrate, by simulation and experiment, the reconstruction algorithm for a 2-D effective attenuation profile from a multiple diffuse reflectance profile.

3.1 *Algorithm and Simulation*

We have built a model to simulate the 2-D diffuse reflectance on a semi-infinite medium that is non-homogeneous on the x-y plane and homogeneous along the z-axis. An example of simulated tissue is shown in Fig. 5(a) with a high absorption crucifixion cross. The simulation and reconstruction procedures are illustrated in Fig. 5. The diffuse reflectance images from eight light sources, which were placed on the boundary of a squared area of 4 cm × 4 cm in size, were simulated by the MC simulation. The resultant 2-D diffuse reflectance images in Fig. 5(b) were then input into our 2-D reconstruction program which treated the image as many 1-D radial lines originating from the point of light source. The outcome was the resolved 2-D effective attenuation profiles as in Fig. 5(c). As shown in Fig. 4, the reconstructed value at a distance smaller than 0.5 cm is invalid and cannot be used. At large r, the simulated light intensity is too small, leading to low signal-to-noise ratio. The diffuse reflectance is a decreasing function and, therefore, if a non-decreasing profile along r is found, it will be treated as an invalid input value. These invalid areas are indicated in black in Fig. 5(c). By combining the resolved profiles of the 8 light-sources by weighted averaging, we obtained the resolved effective attenuation of the whole 4 cm × 4 cm area, as illustrated in Fig. 5(d), which resembles the profile in Fig. 5(a).

The 2-D reconstruction algorithm was repeated on four simulated non-homogeneous semi-infinite tissues of 4 cm × 4 cm in size. These cases were created to see the effects of sharp attenuation change and small object size on the 2-D reconstruction. Figure 6 shows, from top to bottom, the simulation inputs, the resolved effective attenuation profiles and their differences in these four cases. In the input and resolved profiles, the red color on the image represents the area of high effective attenuation, while the blue color represents the area of low effective attenuation. In these simulations, the effective attenuation profile on the x-y plane are shown in Fig. 6(a)–6(d) while it is homogeneous along the depth (z) axis.

In all four cases, the reconstructed 2-D profiles, as illustrated in Fig. 6(e)–6(h), agree well with the corresponding input profiles. The differences between the inputs and the reconstructed profiles are shown in Fig. 6(i)–6(l). Larger differences are found in the regions with abrupt changes in effective attenuation coefficients. It has been observed that the reconstructed profile is low-pass filtered by the diffusion process and therefore, these sharp changes cannot be reconstructed precisely. In Fig. 6(i)–6(l), the error percentage between the input profile and reconstructed profile are shown. In the case of Fig. 6(l), where there is no sharp change in the input profile, the average difference is -1.77% with a standard deviation of 10.8%. With rapid changes present in the profile, the average difference rises to around 22% in both Fig. 6(i) and 6(j). Similarly, a large difference is found in Fig. 4 where there is a sharp edge. The noise in the reconstructed profile is mostly attributable to the limited simulation time and can be reduced by increasing the number of light packets being simulated. The largest difference is exhibited where there is a sharp change in effective attenuation. It has also been observed, that the resolved value of effective attenuation is smaller than the simulated input value when the transport albedo value a' is small, as discussed in Sec. 2.3.

To examine the effect when tissue is non-homogeneous along the depth axis, a series of simulations is carried out. Figure 7 shows the resolved images when the medium in Fig. 6(c) is covered by a thin layer, 0 to 5 mm, of homogeneous tissue with $\mu_a = 0.1\ \text{cm}^{-1}$ and $\mu_s' = 10\ \text{cm}^{-1}$. The resolved value of effective attenuation becomes closer to that of the top homogeneous layer as the thickness of that layer increases. Nevertheless, it demonstrates that even when a thin homogeneous tissue is placed on top of the non-homogeneous medium, the 2-D reconstruction algorithm can still depict the actual pattern based on the diffuse reflectance distribution. As the thickness of the covered layer increases, the resultant pattern fades out and is similar to other diffuse reflectance resolving methods.

3.2 *Imaging Instrument*

Experiments were carried out to test the reconstruction algorithm for the effective attenuation profile on real biological

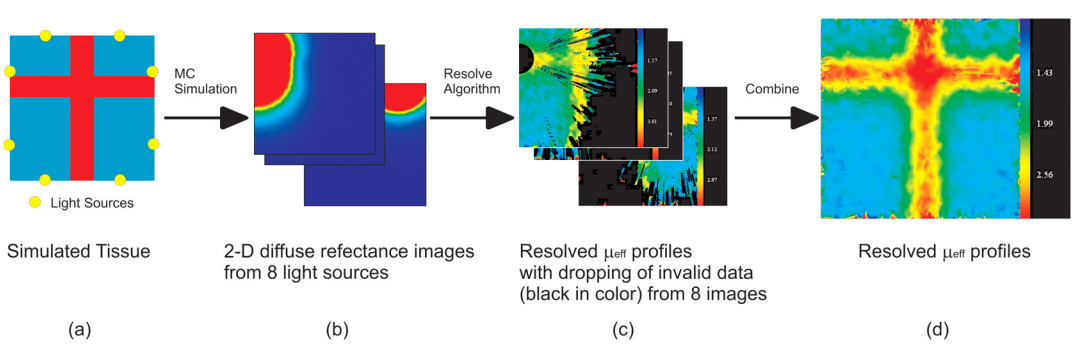

Fig. 5 2-D diffuse reflectance simulation and effective attenuation profile reconstruction.

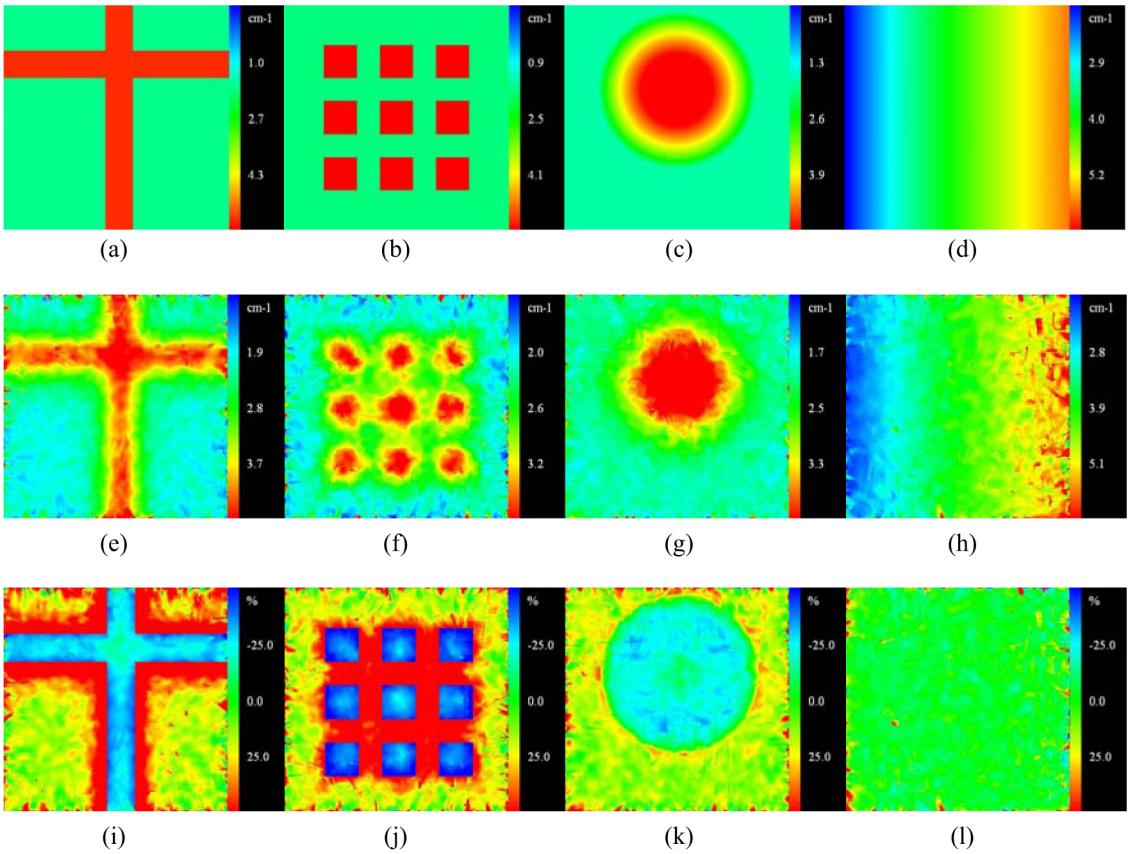

Fig. 6 Simulations on 2-D non-homogeneous media. Top (a), (b), (c), (d) simulated profiles on *x-y* plane; middle (e), (f), (g), (h) reconstructed effective attenuation profiles; bottom (i), (j), (k), (l) differences between the simulated and reconstructed profile.

objects. A commercially available 8-bit monochromic CCD camera was used to capture the 2-D diffuse reflectance images on a flat biological tissue of 4 cm × 4 cm in size. The design of the experiment is illustrated in Fig. 8(a) and will be discussed below.

The LED panel, which was composed of 8 pairs of surface-mount LED light sources, was in direct contact with the tissue under test. An 8-bit monochromic CCD camera, Mightex MCE-B013-U, which had an output image resolution of 1280 × 1024 pixels, was attached to the top. The lens, Computar H0514-MP, attached to the camera had a focal length of 5 mm. The camera was controlled by a personal computer, PC, via USB 2.0 interface. Each pair of LED light sources had two LEDs with central wavelength at 660 and 880 nm respectively, and 3-dB spectral width of approximately 18 nm. The LED panel was controlled by a microcontroller unit through a constant current LED sink driver IC with gain control, Macroblock MBI5170. The PC communicated with the microcontroller via RS232/UART interface to instruct the microcontroller to turn the LEDs on one by one. Since the CCD camera had a relatively low 8-bit gray level, we overcame this limitation by bracketing the exposure time. Five images were captured for each LED, with different exposure values, and they were combined in the PC. The captured images were analyzed by the PC in order for the 2-D effective attenuation profile to be calculated. The design of the LED panel is shown in Fig. 8(b). Eight pairs of 660 and 880-nm surface mount typed LEDs were evenly distributed around the perimeter of the square board. With the effective distance of illumination of each LED being approximately 2 to 3 cm, the LEDs were able to cover the whole area bounded by the square board of the LED panel. The actual number of pixels that covers the 4 cm × 4 cm area was around 760 × 760, which translates to around 19 pixels for each millimeter.

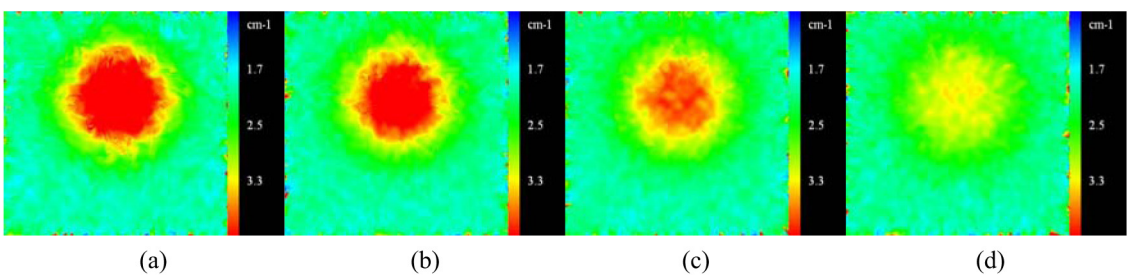

Fig. 7 Resolved effective attenuation profiles with a thin homogeneous layer on top. Thickness of the homogeneous layer: (a) 0 mm, (b) 2 mm, (c) 3.5 mm, and (d) 5 mm.

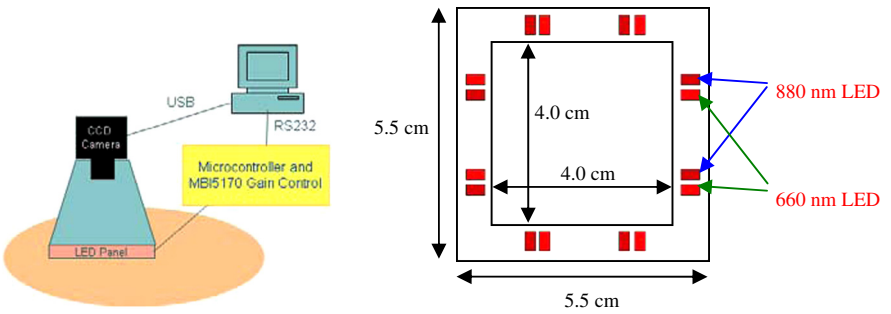

Fig. 8 (a) Imaging Instrument; (b) LED Panel.

3.3 *System Calibration Using Phantom*

A phantom was constructed as in Fig. 9(a) to validate the proposed reconstruction of the effective attenuation profile using the imaging instrument. A piece of solid soap, measuring 9 cm × 9 cm × 4 cm, was used. By using the spatially resolved method in Ref. 7, the absorption and reduced scattering coefficient at 660 nm for the soap were found to be 0.006 and 0.80 cm^{-1}, respectively. As soap is made of fatty acid and alkaline, its optical properties are comparable to that of fat tissue of which the absorption and reduced scattering coefficients were found to be around 0.02 and 1.0 cm^{-1} at 800 nm.[26] A triangular prism was cut off on one side of the soap and the gap was filled with light absorbing mud which has a high absorption coefficient of over 2 cm^{-1}. The aforementioned imaging instrument was placed on the phantom. The captured diffuse reflectance images were analyzed using the proposed algorithm and the reconstructed effective attenuation profile is shown in Fig. 9.

The reconstructed profile in Fig. 9(b) successfully reveals the high absorption area gap. The calculated effective attenuation coefficient value found for the soap was around 0.122 cm^{-1}, which is close to the expected value of 0.120 cm^{-1}. A larger error was found near the tip of the triangular shape due to the low-pass filtering effect of the diffuse process. The result agrees well with the effective attenuation profile of the phantom and the simulation result in Sec. 3.1, thus, demonstrating the feasibility of reconstructing the effective attenuation profile using our imaging instrument. The experiment was repeated and was performed in a darkroom with the room temperature maintained at 25°C throughout the experiment.

3.4 *Preliminary Study on Biological Tissue*

Using the effective attenuation imaging instrument as described, we performed a preliminary study on living tissue. Prior to the experiment on non-homogeneous tissue, the reduced scattering coefficient and absorption coefficient of the skin of our volunteer was found to be 1.33 and 0.09 cm^{-1}, respectively, at 660 nm by using the spatially resolved method in Ref. 7. These numbers translate to an effective attenuation coefficient, μ_{eff}, of 0.62 cm^{-1}. Diffuse reflectance images were captured from the lower leg, using 660-nm LEDs, and were analyzed using the above algorithm. The resultant effective attenuation profile is shown in Fig. 10. The reconstructed effective attenuation profile shows a branch-shaped area with high attenuation corresponding to the veins. The veins are usually near the skin surface. Venous blood contains a high concentration of deoxygenated hemoglobin which leads to a high absorption of red light. The value of μ_{eff} computed for skin tissue, reperesented by a blue area in Fig. 10, is around 0.64 cm^{-1}, whereas, it is about 2.0 cm^{-1} for the vein. The μ_{eff} is close to the aforementioned result obtained from the spatially resolved method. The black color in Fig. 10 indicates that the pixel

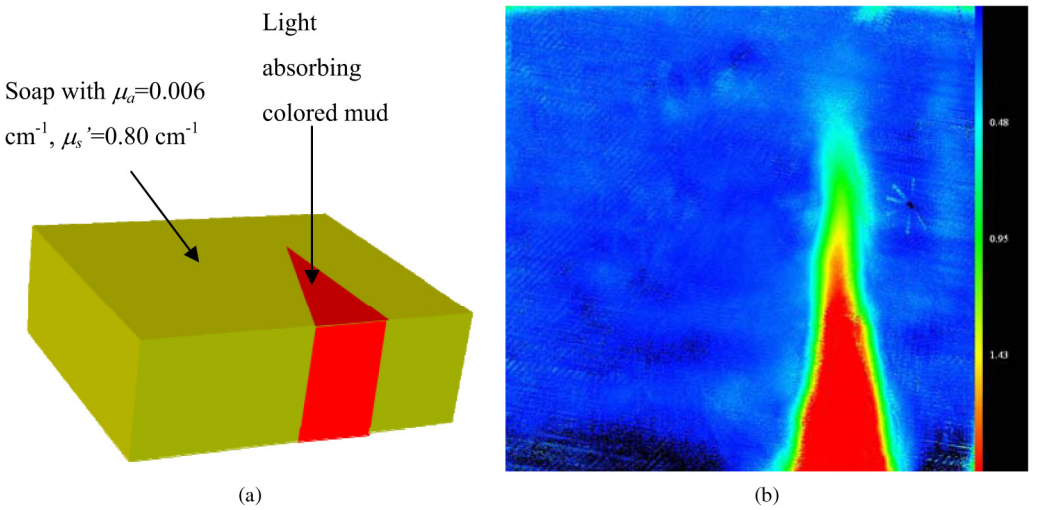

Fig. 9 (a) Phantom structure; (b) resolved effective attenuation profile.

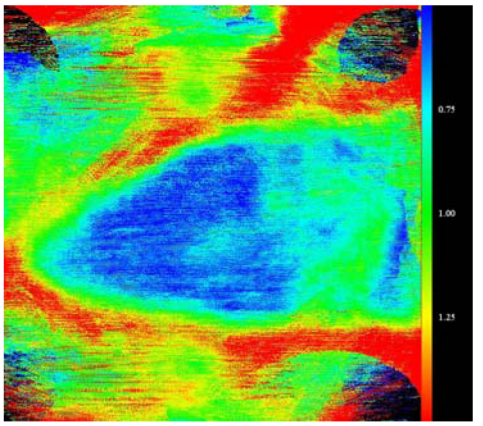

Fig. 10 Resolved effective attenuation profile of skin tissue.

reading of that particular point is not valid under the reconstruction algorithm, as described in Sec. 3.1. The area in black can be reduced by increasing the number of light sources, optimizing the placement of the light source, or increasing the exposure bracketing per light source. There are some horizontal artifacts on the resultant image caused by the CCD noise that occurs when capturing with high gain factor. Compared to the previous spatially resolved studies, our resolved algorithm is able to provide a highly detailed 2-D effective attenuation profile.[11] The reconstruction algorithm takes about 200 sec to resolve the effective attenuation profile on a 2.4-GHz single-core PC, and the resolution for the image is 20 pixels per millimeter. The processing time can be drastically reduced to 3 or 4 sec when the resolution of the image is reduced to 2 pixels per millimeter, a higher resolution compared to that in Ref. 11.

4 Discussion

Imaging based on diffuse optics can be used in many biological studies. Medical imaging techniques such as ultrasonography, computed tomography (CT) and magnetic resonance imaging (MRI) provides detailed image on tissue density, whereas, infrared thermography and Doppler imaging garners information on heat distribution and blood flow in living bodies. Distinct from those, diffuse optical imaging gives information on optical absorption by optical spectroscopy and it can be used for identifying the chemical composition of biological tissue. Our proposed algorithm produces a high temporal and spatial resolution on the effective attenuation properties. Compared to previous work on spatially resolved spectroscopy, our scheme can resolve millimeter sized objects such as blood vessels and tumors. Unlike DOT and modulated imaging, our scheme targets 2-D reconstruction. Therefore the computational complexity and the number of captured images required per measurement are much reduced. As a result, the processing and capturing time can be greatly reduced as well. Furthermore, our method can be implemented at a low cost, as only a fixed point light source and a simple capturing device are used over the monitoring area.

To the best of our knowledge, this paper is the first study aimed at achieving high spatial resolution reconstruction of μ_{eff} from the spatial diffuse reflectance curve. We use a simplified empirical model for the diffuse reflectance to achieve high resolution spatial reconstruction, unlike DOT which requires a more complex procedure to solve the diffusion equation as in Ref. 24. Simultaneous reconstruction of μ_a and μ_s' is made possible with the use of frequency resolved or time-resolved measurement.[12,13] In the spatially resolved system, the diffusion coefficient D and the effective attenuation coefficient μ_{eff} can be resolved by the measurement of diffuse reflectance on a homogeneous medium.[7] With regards to a non-homogeneous medium, there is still no efficient solution to resolve D and μ_{eff} simultaneously without time or frequency response information. Therefore, a 2-D spatially resolved system is usually assumed to have a constant D based on the $\mu_s' \gg \mu_a$ assumption in the radiative transfer equation.[21] To obtain the 2-D absorption coefficient profile using the spatially resolved system, the common practice is to assume constant μ_s' or D such that μ_a can be deduced from μ_{eff}.[11,19,20] There are, however, some limitations on the proposed method. Firstly, the reconstruction algorithm is based on the assumptions of large transport albedo a', as shown in Eq. (1), and the fixed value of k_2. It can be seen in Figs. 3 and 4, that variation in a' in a homogeneous profile may lead to errors in the resolved μ_{eff} profile due to the fixed k_2 value in our reconstruction. It is also found, that k_2 tends to be larger with a small r, < 1.5 cm, and vice versa. Further study on the correlation between k_2 revealed that a' and r will be required to minimize this error. In this paper, r is not greater than 4 cm and a' is larger than 0.95, therefore, constant k_2 is assumed for simplicity. Secondly, the intrinsic low pass filtering characteristic from the diffusion process has limited the spatial resolution. Sub-millimeter spatial resolution is not feasible as the information is eliminated by the diffusion process, however, by processing images with less pixel density, it allows a higher temporal resolution. Thirdly, our algorithm is not targeted for resolving the depth axis, z-axis, information, but to improve the 2-D spatial and temporal resolutions. To solve the effective attenuation profile in 3-D, a more sophisticated light source, more captured data, and more complicated resolve algorithms would be required meaning that the temporal resolution could be greatly limited. In the cases of DOT and modulated imaging, the former needs a scanning light source and the latter uses spatially modulated illumination.

In this paper, we have demonstrated the use of a low cost camera on a flat, biological subject to resolve the effective attenuation profile. The imaging instrument is simple and cost effective. The drawback is that a longer capturing time is needed with the use of a less sensitive camera and more images with different exposure settings are required to compensate for the decreased sensitivity in a low light situation. If a thermoelectric-cooled 16-bit camera as in DOT is used, the capturing time can be reduced.[19] In addition, the image quality can be enhanced by using high sensitivity cameras. The computing time can also be further optimized by controlling the resolution and reducing the intermittent calculation. Despite not being able to achieve 3-D reconstruction with the use of eight point light sources, the reduced 2-D projection of the tissue absorption can still provide some useful information on non-homogeneous structures such as tumors and wounds. Furthermore, the low computational complexity of the algorithm allows the technique to be applied in real-time applications such as breast cancer detection, muscle oxygenation distribution and functional brain imaging.

5 Conclusion

We have proposed a fast and simple reconstruction scheme for the 2-D effective attenuation profile in high resolution based on diffuse reflectance measurement. We have demonstrated that we can obtain the local values of the effective

attenuation coefficient by simply calculating the first derivative of the spatial diffuse reflectance rather than solving the diffusion equation. With the simplified diffuse approximation model, we have shown the reconstruction of effective attenuation profiles for different non-homogeneous media by simulations and experiments. The reconstructed profiles revealed the non-homogeneous pattern in the simulations and experiments using the phantom.

References

1. P. N. Prasad, *Introduction to Biophotonics*, John Wiley & Sons, Inc., Hoboken, New Jersey (2003).
2. H. Liu et al., "Noninvasive investigation of blood oxygenation dynamics of tumors by near-infrared spectroscopy," *Appl. Opt.* **39**(28), 5231–5243 (2000).
3. N. H. Kashou, R. Xu, and C. J. Roberts, "Using FMRI and FNIRS for localization and monitoring of visual cortex activities," *IEEE Engineering in Medicine and Biology Society*, Lyon, pp. 2634–3638 (2007).
4. M. Xu et al., "NIRS measurement of hemodynamic evoked responses in the primary somatosensory cortex by finger stimulation," *IEEE Conference on Complex Medical Engineering*, Beijing, pp. 1425–1429 (2007).
5. D. Arifler et al., "Spatially resolved reflectance spectroscopy for diagnosis of cervical precancer: Monte Carlo modeling and comparison to clinical measurements," *J. Biomed. Opt.* **11**(6), 064027 (2006).
6. S. A. Prahl et al., "A Monte Carlo model of light propagation in tissue," *Proc. SPIE*, **IS 5**, 102–111 (1989).
7. T. J. Farrell, M. S. Patterson, and B. Wilson, "A diffusion theory model of spatially resolved, steady-state diffuse reflectance for the noninvasive determination of tissue optical properties in vivo," *Med. Phys.* **19**(4), 879–888 (1992).
8. D. E. Hyde et al., "A diffusion theory model of spatially resolved fluorescence from depth-dependent fluorophore concentrations," *IOP Phys. Med. Biol.* **46**(2), 369–383 (2001).
9. L. Gobin, L. Blanchot, and H. Saint-Jalmes, "Integrating the digitized backscattered image to measure absorption and reduced-scattering coefficients in vivo," *Appl. Opt.* **38**(19), 4217–4227 (1999).
10. M. Pilz, S. Honold, and A. Kienle, "Determination of the optical properties of turbid media by measurements of the spatially resolved reflectance considering the point-spread function of the camera system," *J. Biomed. Opt.* **13**(5), 054047 (2008).
11. K. J. Kek et al., "Optical imaging instrument for muscle oxygenation based on spatially resolved spectroscopy," *Opt. Express* **16**(22), 18173–18187 (2008).
12. M. S. Patterson, B. Chance, and B. C. Wilson, "Time resolved reflectance and transmittance for the non-invasive measurement of tissue optical properties," *Appl. Opt.* **28**(12), 2331–2336 (1989).
13. W. Becker et al., "Advanced time-correlated single photon counting technique for spectroscopy and imaging in biomedical systems," *Proc. SPIE*, **5340**, 104–112 (2004).
14. R. X. Xu et al., "Development of a handheld near-infrared imager for dynamic characterization of in vivo biological tissue systems," *Appl. Opt.* **46**(30), 7442–7451 (2007).
15. D. E. Hyde et al., "A diffusion theory model of spatially resolved fluorescence from depth-dependent fluorophore concentrations," *Phys. Med. Biol.* **46**(2), 369–383 (2001).
16. B. S. Sorg et al., "Spectral imaging facilitates visualization and measurements of unstable and abnormal microvascular oxygen transport in tumors," *J. Biomed. Opt.* **13**(1), 014026 (2008).
17. V. P. Zharov et al., "Infrared imaging of subcutaneous veins," *Lasers Surg. Med.* **34**(1), 56–61 (2004).
18. V. Paquit et al., "Combining near-infrared illuminants to optimize venous imaging," *Proc. SPIE* **6509**, 65090H (2007).
19. S. D. Konecky et al., "Imaging complex structures with diffuse light," *Opt. Express* **16**(7), 5048–5060 (2008).
20. D. J. Cuccia et al., "Modulated imaging: quantitative analysis and tomography of turbid media in the spatial-frequency domain," *Opt. Lett.* **30**(11), 1354–1356 (2005).
21. L. V. Wang and H.-I. Wu, *Biomedical Optics: Principles and Imaging*, John Wiley & Sons, Inc., Hoboken, New Jersey (2007).
22. S. P. Lin et al., "Measurement of tissue optical properties by the use of oblique-incidence optical fiber reflectometry," *Appl. Opt.* **36**(1), 136–143 (1997).
23. L. V. Wang, S. L. Jacques, and L. Q. Zheng, "Conv—convolution for responses to a finite diameter photon beam incident on multi-layered tissues," *Comput. Methods Prog. Biomed.* **54**(3), 141–150 (1997).
24. V. A. Markel and J. C. Schotland, "Inverse problem in optical diffusion tomography. Role II of boundary conditions," *J. Opt. Soc. Am. A* **19**(3), 558–566 (2002).
25. R. A. J. Groenhuis, H. A. Ferwerda, and J. J. Ten Bosch, "Scattering and absorption of turbid materials determined from reflection measurements. 1: theory," *Appl. Opt.* **22**(16), 2456–2462 (1983).
26. G. Mitic et al., "Time-gated transillumination of biological tissues and tissue like phantoms," *Appl. Opt.* **33**(28), 6699–6710 (1994).